

Faceting–roughening of twin grain boundaries

**B. B. Straumal, B. Baretzky,
O. A. Kogtenkova, A. S. Gornakova &
V. G. Sursaeva**

Journal of Materials Science

Full Set - Includes 'Journal of Materials
Science Letters'

ISSN 0022-2461

Volume 47

Number 4

J Mater Sci (2012) 47:1641-1646

DOI 10.1007/s10853-011-5807-y



Your article is protected by copyright and all rights are held exclusively by Springer Science+Business Media, LLC. This e-offprint is for personal use only and shall not be self-archived in electronic repositories. If you wish to self-archive your work, please use the accepted author's version for posting to your own website or your institution's repository. You may further deposit the accepted author's version on a funder's repository at a funder's request, provided it is not made publicly available until 12 months after publication.

Faceting–roughening of twin grain boundaries

B. B. Straumal · B. Baretzky · O. A. Kogtenkova ·
A. S. Gornakova · V. G. Sursaeva

Received: 9 May 2011 / Accepted: 19 July 2011 / Published online: 2 August 2011
© Springer Science+Business Media, LLC 2011

Abstract The coincidence site lattice (CSL) plays a similar role for grain boundaries (GB) as the crystal lattice plays for free surfaces. The most densely packed CSL is the twin-related CSL, characterized by an inverse density of coincidence sites $\Sigma = 3$. Phase diagrams in coordinates “relative temperature T/T_m —misorientation angle θ —inclination angle φ ” were constructed for the twin GBs in Cu, Al, and Mo having different stacking fault energy γ . At low γ the twin GB remains faceted at all φ values and the number of crystallographically different facets increases with decreasing temperature. With increasing γ asymmetric twin GBs become more and more rough, and fewer facets appear with decreasing temperature. Also, with increasing γ the facets start to degenerate of into the first order rough-to-rough ridges. The behavior of twin GBs in Cu, Al, and Mo is compared with that of twin GBs in Zn.

Introduction

High-angle grain boundaries are characterized by a misorientation angle θ above 15° . They cannot be described as an array of lattice dislocations since at high θ the

dislocation cores merge. At certain misorientations θ_Σ called coincidence misorientations a part of the lattice sites of the lattice 1 coincide with the lattice sites of the lattice 2 forming a coincidence sites lattice (CSL) [1]. A CSL is characterized by a parameter Σ (Σ is the inverse density of coincidence sites). At θ_Σ GBs have a perfect periodic structure. These coincidence GBs have in many cases low energy σ_{GB} (see review [2] and references therein), migration rate [3–6], diffusion permeability [7–9], high strength (monograph [10] and references therein) and other extreme properties. Coincidence GBs also tend to facet. In other words, a curved GB breaks into an array of flat segments. These segments are usually parallel to the densely packed planes in the CSL. Strictly speaking, a CSL exists only exactly at θ_Σ . Any small deviation $\Delta\theta = |\theta - \theta_\Sigma|$ destroys the geometrical coincidence of lattice sites. However, physically a GB tends to conserve its low-energy structure up to a certain critical value θ_c . The structure of such (special) GBs consists of portions of perfectly coincident lattices separated by intrinsic GB dislocations (IGBDs) [11]. The IGBDs have a Burgers vector b_Σ which is shorter than that of lattice dislocations $b:b_\Sigma = b \Sigma^{-2}$. It has been demonstrated that special GBs conserve their special structure and properties up to a certain critical misorientation $\Delta\theta_c$ and temperature T_c [12]. Special properties mean that close to θ_Σ the GBs possess minimal energy, mobility, diffusivity, etc. [2–9, 13, 14]. $\Delta\theta_c$ decreases exponentially and T_c decreases parabolically with increasing Σ [12]. In other words, with decreasing temperature an increasing number of GBs exhibit special structures and properties.

The physical reason for such a behavior is the GB faceting–roughening phase transformation similar to that of free surfaces [15–18]. The energy of individual steps in a flat surface facet decreases with increasing temperature.

B. B. Straumal (✉) · O. A. Kogtenkova ·
A. S. Gornakova · V. G. Sursaeva
Institute of Solid State Physics, Russian Academy of Sciences,
Chernogolovka, Russia 142432
e-mail: straumal@issp.ac.ru; straumal@mf.mpg.de

B. B. Straumal · B. Baretzky
Karlsruher Institut für Technologie, Institut für Nanotechnologie,
Hermann-von-Helmholtz-Platz 1,
76344 Eggenstein-Leopoldshafen, Germany

At a certain temperature T_R the step energy becomes zero. If $T_R < T_m$ (T_m is the melting temperature) the flat facet cannot be stable above T_R due to the spontaneous formation of step arrays and becomes rough (roughening transition) [18]. A GB roughening transition of second order has been observed recently [19]. It has been predicted theoretically that that T_R is lower for the facets with higher step energy (i.e., for the facets less densely packed with lattice sites) [18]. Experimentally a sequence of three roughening transitions for different surface facets at different T_R has been observed only in solid helium [20].

The shape of special GB area was experimentally constructed for the $\Sigma = 17$ GB in Sn [21]. It has been observed that the introduction of lattice dislocations by increase of second tilt or twist misorientations [22] or increasing impurity content [23] decreases the T_C . For the construction of “ T - θ ”, “ T_C - Σ ”, and “ $\Delta\theta$ - $\ln\Sigma$ ” plots in [12] the data for different metals, semiconductors and oxides were used. On the one hand, it means that the decrease of $\Delta\theta$ and T_C with increasing Σ is a rather general phenomenon. On the other hand, it is clear that the shape of faceting/roughening diagrams for the same Σ should be different in different materials. GBs with $\Sigma = 3$ are called twins, and play an exclusive role in the metallic alloys [24, 25]. In many cases twin GBs form the majority of the GB population in polycrystals like, for example, in nano-grained materials after severe plastic deformation [26]. Almost always twin GBs appear faceted in metallic alloys [27]. Straight parallel couples of these GBs gave them their special name in many different languages (twin, Zwilling, macle, двойник) [28]. In this study we will compare the “misorientation θ —inclination φ ” phase diagrams for $\Sigma = 3$ GBs in metals with different stacking fault energy (Cu, Al, Mo, and Zn).

Experimental

For the investigation of GB faceting the Cu, Al, Mo, and Zn bicrystals were grown using the modified Bridgman technique [16–21, 29–34]. In the Cu and Mo bicrystals the cylindrical central grain was completely surrounded by the external cylindrical grain forming a $\Sigma 3 \langle 110 \rangle$ tilt grain boundary [31, 33, 35, 36]. In the Al both grains were semi-cylindrical [32, 37, 38]. In case of Al one bicrystal had an exact coincidence tilt grain boundary $\Sigma 3 \langle 110 \rangle$. A second bicrystal [32] had a GB with a misorientation of $\Delta\theta = 3^\circ$ degrees from $\Sigma 3 \langle 110 \rangle$. In Zn bicrystals the grain was semi-surrounded by grain 1 forming a $[10\bar{1}0]$ twin tilt grain boundary. Scanning electron microscopy, light microscopy, and electron back-scattering diffraction (EBSD) was used to characterize the shape of GBs in as-grown

bicrystals and after annealing in vacuum or in argon at various temperatures (Fig. 1). In case of Zn, the shape of the migrating GB loop was studied in situ in a hot stage of a light microscope using polarized light. In case of Al the equilibrium GB shape was calculated using the Wulff approach and the measured values of GB energy for different facets [32, 37, 38]. For this purpose the bicrystalline samples were coated with a layer of Sn–Al alloy and annealed in Ar gas atmosphere at a pressure of 2×10^{-4} Pa and different temperatures. Then the contact angle α between GB and quenched solid/liquid interface for various GB inclination angles φ , and geometry of facets was recorded in bright and dark field in the light microscope and measured. The ratio of GB energy σ_{GB} to solid/liquid interface energy σ_{SL} was calculated using the values of measured contact angle α : $\sigma_{GB} = 2\sigma_{SL} \cos(\alpha/2)$.

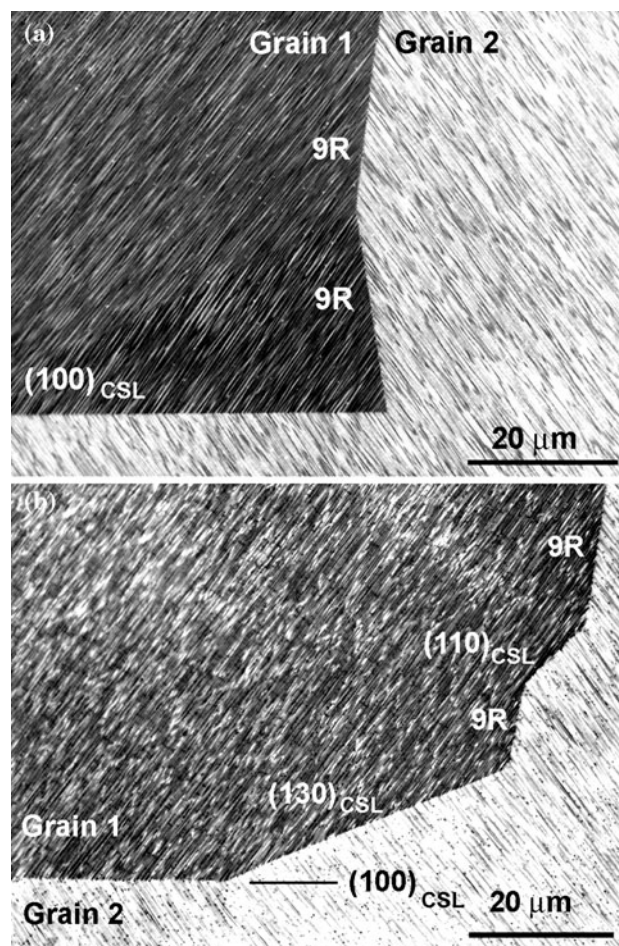


Fig. 1 Light micrographs of faceted $\Sigma 3$ GB ($\Delta\theta = 0$) in Cu $\{110\}$ bicrystal after annealing at **a** 800 °C and **b** 400 °C. The common $\{110\}$ axis is perpendicular to the sample (and figure) plane. The positions of various facets are shown

Results and discussion

Faceting of $\Sigma = 3$ twin GB in copper. First order facet-to-facet ridges

Copper possesses a low stacking fault energy of $\gamma = 55 \text{ mJ/m}^2$ [39]. The measurements of a stacking fault energy are usually based on the dislocations structure and properties. The structure of a stacking fault in face-centred cubic (fcc) metals is the same as that of symmetric $\Sigma = 3$ twin GBs (STGBs), i.e., that of plain $\Sigma = 3$ GB which is parallel to the (111) most closely packed planes in both grains. In Fig. 2 the three-dimensional phase diagram for the $\Sigma = 3$ twin GBs in Cu is shown in the “Relative temperature T/T_m —misorientation angle θ —inclination angle φ ” coordinates (T being the annealing temperature, T_m being the melting temperature of Cu). Zero value of inclination angle $\varphi = 0$ corresponds to the symmetric twin GB. There is a huge number of papers where the faceting of symmetric twins in pure Cu was observed up to the melting temperature (some of these papers are [30, 31, 35, 36, 40–45]). It means that the roughening does not take place for the symmetric $\Sigma = 3$ twin GBs up to the melting point (Fig. 1a). The misorientation interval $\Delta\theta = |\theta - \theta_{\Sigma 3}|$ where the $\Sigma = 3$ twin GBs remain faceted is finite and very broad [12]. In case of copper the direct evidence exists for the faceting of symmetric $\Sigma = 3$ twin GBs up to $\Delta\theta = 2^\circ$. The indirect evidence from rotating single crystal balls experiments gives the $\Delta\theta > 4^\circ$ [46]. For $\Delta\theta < 2^\circ$ the thermal grooving experiments gave the dependence of the GB energy σ_{GB} on θ and permitted to construct respective

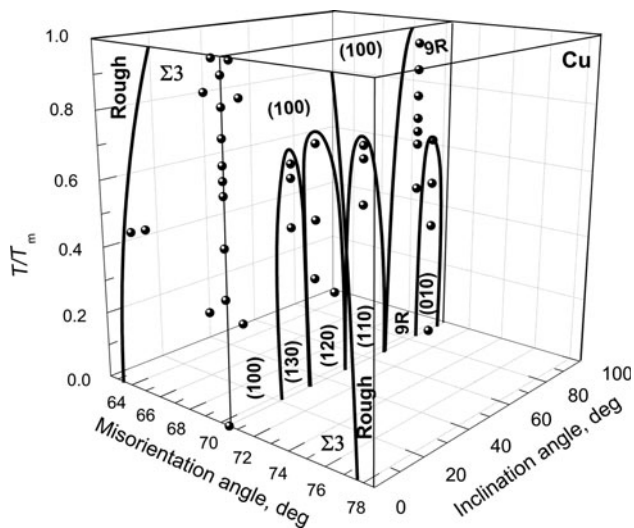


Fig. 2 Three-dimensional phase diagram for the $\Sigma = 3$ twin GBs in Cu in the “Relative temperature T/T_m —misorientation angle θ —inclination angle φ ” coordinates (T being the annealing temperature, T_m being the melting temperature of Cu). Zero value of inclination angle $\varphi = 0$ corresponds to the symmetric twin GB

Wulff plots [36]. It has to be underlined that the phase diagram in Fig. 2 concerns only high-purity copper, since the addition of impurities can drastically change the faceting behavior of $\Sigma = 3$ twin GBs in copper [40–42].

At $\Delta\theta = 0 \pm 1^\circ$ the $\Sigma = 3$ twin GB in copper remains faceted up to the melting temperature at all values of inclination angle φ (Fig. 2) [31, 35, 41]. No rounded edges between facets were observed up to $0.95 T_m$ [31, 35]. At $T = 0.95 T_m$ (i.e., very close to the melting temperature) only two facets appear at the $\Sigma 3$ GB: $(100)_{CSL}$ and $9R$. The $(100)_{CSL}$ plane is a symmetric twin GB which is parallel to the (111) planes in both fcc grains. At high temperatures the twins in Cu are not rectangular (Fig. 1a) unlike those in Au [47]. The facets at the end of twin plates form an angle of 82° with the $(100)_{CSL}$ plane (Fig. 1a). This 82° facet does not correspond to any low-index CSL plane. The minimum of $\sigma_{GB}(\theta)$ at 82° is due to the formation of a thin GB layer with the so-called $9R$ structure, forming a plate of bcc GB phase in the fcc matrix [48–50]. The $(100)_{CSL}/82^\circ 9R$ edges of the twin plates are sharp (Fig. 1) forming so-called first order facet-to-facet ridges [51]. This suggests that facets $(100)_{CSL}$ and $9R$ in pure Cu remain stable up to the melting temperature T_m , and their roughening temperatures $T_R[(100)_{CSL}]$ and $T_R[9R]$ are higher than T_m .

By decreasing the temperature new facets with lower density of coincidence sites appear in $\Sigma = 3$ GBs at various φ (Figs. 1 and 2). These additional facets are $(010)_{CSL}$, $(110)_{CSL}$, $(120)_{CSL}$, and $(130)_{CSL}$ (Fig. 1b). All of them are less densely packed CSL facets than $(100)_{CSL}$. However, they have lower density of coincidence sites. The lower density of coincidence sites corresponds to the lower height of elementary step in the GB plane. At $T = 0.5 T_m$ six crystallographically different facets exist simultaneously for $\Sigma 3$ GB (Fig. 1b). All observed edges between the facets are sharp (Fig. 1b). Hence, the new facets appear not at rough, rounded parts of the GB, as observed for surface facets in Pb, Au or He [30, 52, 53], but at the sharp edges between existing facets. It means that the temperature T_{Rf} when a less densely packed CSL facet really appears in equilibrium shape of a GB is lower than true roughening temperature T_R for this facet. Since all $\Sigma 3$ GBs studied were completely faceted, no fields corresponding to the rough phases are present in the $\Delta\theta = 0$ plane of the phase diagram in Fig. 2. The existence areas corresponding to the $(110)_{CSL}$, $(120)_{CSL}$, and $(130)_{CSL}$ facets are surrounded by the area of the $(100)_{CSL}$ facet. The existence areas of the $(010)_{CSL}$ facets is surrounded by the area of the $9R$ facet.

Faceting of $\Sigma = 3$ twin GB in aluminum. First order facet-to-rough ridges

The stacking fault energy of Al $\gamma = 166 \text{ mJ/m}^2$ [54] is much higher than that of Cu. In Fig. 3 the

three-dimensional phase diagram for the $\Sigma = 3$ twin GBs in Al is shown in the “ $T/T_m - \theta - \varphi$ ” coordinates. We did not find in the literature any evidence that the faceting of $\Sigma = 3$ twin GBs in Al can be observed above $\Delta\theta = |\theta - \theta_{\Sigma 3}| = 2^\circ$ [55]. In our experiments with Al bicrystals having $\Delta\theta = 3^\circ$ the short portion of the $(100)_{\text{CSL}}$ facet contacted with rough rounded portions of $\Sigma = 3$ GB [32, 38]. It means that the angular interval of the existence of special $\Sigma = 3$ GB in Al is much narrower than that in Cu. As seen in Fig. 3a, at $\Delta\theta = 0$ the $\Sigma = 3$ twin GBs in Al is completely faceted [37, 38]. Close to the melting temperature two facets exist at the $\Sigma 3$ GB: $(100)_{\text{CSL}}$ and $9R$, similar to Cu. However, the $9R$ non-CSL facet disappears with decreasing temperature already at $0.8 T_m$. The $(010)_{\text{CSL}}$ facet appears instead along with the $(110)_{\text{CSL}}$ facet. Thus, below $T/T_m = 0.8$ only three crystallographically

different facets (namely $(100)_{\text{CSL}}$, $(010)_{\text{CSL}}$, and $(110)_{\text{CSL}}$) exist in Al, and not six as in Cu. In Fig. 3b the “ $T/T_m - \Delta\theta = 3^\circ - \varphi$ ” section is shown. It is superposed on the “ $T/T_m - \theta = \theta_{\Sigma 3} - \varphi$ ” section shown in Fig. 3a. It is clearly seen that only one $(100)_{\text{CSL}}$ facet surrounded by the rough rounded GB portion is present in the Al bicrystal with $\Delta\theta = |\theta - \theta_{\Sigma 3}| = 3^\circ$. Therefore, the existence area of the $\Sigma = 3$ twin GBs in Al is much narrower than that in Cu. The contact between facets and rough GB portions has a slope discontinuity (i.e., of first order) like on the surface of Au [39]. The facet and rounded rough GB portions form the first-order facet-to-rough GB ridges. The number of various CSL-facets at low temperatures is also less than in Cu.

Faceting of $\Sigma = 3$ twin GB in molybdenum. Second order facet-to-rough and first order rough-to-rough ridges

The stacking fault energy of Mo $\gamma = 410 \text{ mJ/m}^2$ [56] is much higher than that of Cu and Al. In Fig. 4 the three-dimensional phase diagram for the $\Sigma = 3$ twin GBs in Mo is shown in the “ $T/T_m - \theta - \varphi$ ” coordinates. We did not find in the literature any evidence that the faceting of $\Sigma = 3$ twin GBs in Mo can be observed above $\Delta\theta = |\theta - \theta_{\Sigma 3}| = \pm 0.5^\circ$ [57]. The circular $\Sigma = 3$ twin GB in a Mo bicrystal contains only two parallel flat facets, namely $(111)_1 \parallel (111)_2$ STGBs or $(100)_{\text{CSL}}$ facets [33]. Both flat $(100)_{\text{CSL}}$ facets contact with rounded rough GB portions. This fact is reflected in Fig. 4. The existence area of $(100)_{\text{CSL}}$ facet is surrounded by the rough GB area. The flat $(100)_{\text{CSL}}$ facets form smooth edges (no slope discontinuity)

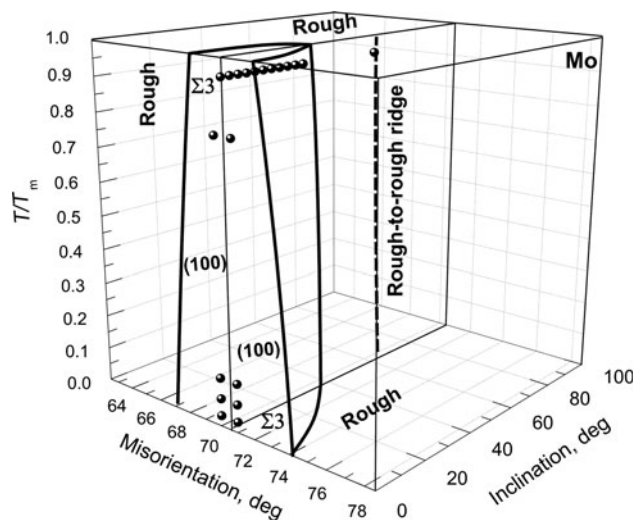
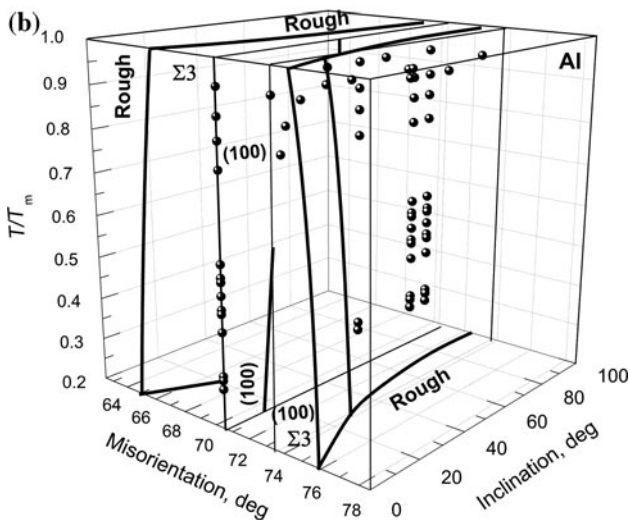
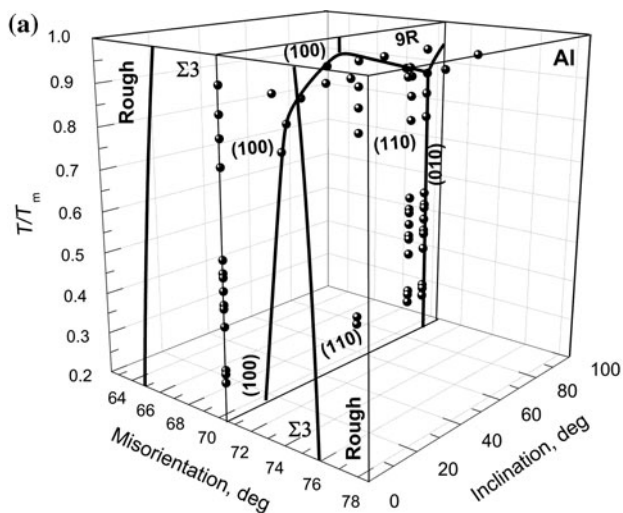


Fig. 3 Three-dimensional phase diagram for the $\Sigma = 3$ twin GBs in Al in the “Relative temperature T/T_m —misorientation angle θ —inclination angle φ ” coordinates. **a** $\theta = \theta_{\Sigma 3}$. **b** same as Fig. 3a with added data for $|\theta - \theta_{\Sigma 3}| = 3^\circ$

Fig. 4 Three-dimensional phase diagram for the $\Sigma = 3$ twin GBs in Mo in the “Relative temperature T/T_m —misorientation angle θ —inclination angle φ ” coordinates. Vertical dotted line at $\theta = \theta_{\Sigma 3}$, $\varphi = 60$ marks the position of the first order rough-to-rough ridge

with rounded rough GB portions. This roughening behavior is similar to that of facets on the surface of small lead balls [53]. The rough GBs curve away from the plane of the $(100)_{\text{CSL}}$ facets as x^β with $\beta = 1.69 \pm 0.07$ on one side and $\beta = 1.72 \pm 0.07$ on the other side of a facet. Therefore, GB roughening belongs to the Pokrovsky-Talapov universality class.

Four slope discontinuities between two rounded rough GB portions were also observed. All of them are in the same crystallographic position and are shown in Fig. 4 by one vertical line at $\varphi = 60^\circ$ [33]. This was the first experimental observation of the first-order rough-to-rough ridges theoretically predicted by the Davidson and den Nijs model [58, 59]. Therefore, GBs allow one to observe a broad diversity of faceting/roughening phenomena which is quite different and complementary to that of faceting/roughening of free surfaces [60, 61].

Faceting of twin GB in zinc

The stacking fault energy of zinc $\gamma = 140 \text{ mJ/m}^2$ [62] is much higher than that of copper and lower than that of aluminum and molybdenum. However, crystallographically the twins in zinc are very different from $\Sigma = 3$ twins in Cu, Al, and/or Mo. It is because the ideal CSLs does not exist in Zn, and the approach of CCSL has to be used instead [63, 64]. The parallel elongated sides of the twin plate are formed by the coherent symmetric twin $(1\bar{1}0\bar{2})_1 \parallel (1\bar{1}0\bar{2})_2$ grain boundary (STGB) facets [34]. The faceting/roughening behavior is twin GBs in zinc is quite different in comparison with fcc counterparts. On the one hand, the $(1\bar{1}0\bar{2})_1 \parallel (1\bar{1}0\bar{2})_2$ STGB in Zn remains faceted up to T_m , similar to $(111)_1 \parallel (111)_2$ STGB in Cu, Al, and Mo. Moreover, the GB half loop between two parallel symmetric portions of twin GB become completely rounded (rough) at T_R which is very close to T_m . This behavior is very similar to that of Al. Remember that the stacking fault energy of zinc is also close to that of Al. On the other hand, below the roughening temperature T_R the faceting of asymmetric twin GBs in zinc (twin tip) differs a lot from that of Cu, Al, and Mo. Below 360°C the twin tip contains only one plane facet 1 which is nearly parallel to the $(\bar{1}10\bar{2})_2$ plane and has the angle of 84° with the coherent STGB. Above 360°C the second facet 2 appears at the tip of the twin plate. This facet is nearly parallel to the $(\bar{1}100)_1$ plane and has the angle of 46° with the coherent STGB. Between 360 and 410°C both 84° and 46° facets coexist, and 84° facet gradually disappear with increasing temperature. Above 410°C only 46° facet is present in the twin tip [34].

Similar to Mo, we also observed in Zn how two first-order facet-to-rough ridges separated by a GB facet merge together with increasing temperature and form a first-order

rough-to-rough GB ridge [51, 65]. This phenomenon was observed in tilt $[10\bar{1}0]$ GB with $\theta = 30^\circ$. At low temperatures a GB loop has a facet dividing two first-order facet-to-rough ridges. This facet is parallel to the closely packed plane of a constrained coincidence sites lattice (CCSL) for the $30^\circ [10\bar{1}0]$. The c/a value is irrational in Zn, a being the lattice spacing in the basal plane (0001) and c being the lattice spacing in the direction perpendicular to the (0001) plane. Therefore, the exact CSL exists in Zn only for GBs with rotation around [0001] axis. In all other cases the so-called constrained coincidence sites lattice approach should be used [63, 64]. It is interesting that the tangents to the rough GB portions in the end-points of the facet are also parallel to closely packed CCSL planes. By increasing temperature the facet between points disappears, and the first-order rough-to-rough GB ridge form instead of two first-order facet-to-rough GB ridges. However, the orientation of the first-order rough-to-rough GB ridge is not arbitrary. The tangents to the rough GB portions in the ridge point remain parallel to the to closely packed CCSL planes [51, 65].

Conclusions

- GB faceting/roughening is the physical reason for the “special GB—general GB” phase transitions;
- GBs allow one to observe a broad diversity of faceting/roughening phenomena which is quite different and complementary to that of faceting/roughening of free surfaces;
- New facets with lower density of coincidence sites (in other words, with lower height of elementary step) continuously appear by decreasing temperature;
- With increasing stacking fault energy the twin GBs contain fewer facets, the asymmetric twin GBs become rough at T/T_m ;
- With increasing stacking fault energy the facets tend to degenerate of into the first order rough-to-rough ridges.

Acknowledgements Authors thank the Russian Foundation for Basic Research (contract 09-03-92481) and Israel Ministry of Science (project 3-5790) and the Program of bilateral cooperation between Russian and Polish Academies of Sciences for the financial support. Authors cordially thank Prof. E. Rabkin, Prof. R. Valiev, Prof. T. Langdon, and Dr. A. Mazilkin for stimulating discussions, Mr. A. Nekrasov for the help with SEM and EPMA measurements.

References

1. Grimmer H, Bollmann W, Warrington DT (1974) Acta Cryst A 30:197
2. Sutton AP, Balluffi RW (1987) Acta Metall 35:2177

3. Rutter JW, Aust (1965) *Acta Metall* 13:181
4. Fridman EM, Kopecky CV, Shvindlerman LS (1975) *Zt Metallkde* 66:533
5. Aristov VY, Kopecky CV, Shvindlerman LS (1977) *Scr Metall* 11:109
6. Antonov AV, Kopecky CV, Shvindlerman LS (1971) *Phys Metall Metallogr* 32:187
7. Aleshin AN, Aristov VY, Bokstein BS et al (1978) *Phys Stat Sol A* 45:359
8. Aleshin AN, Bokstein BS, Shvindlerman LS et al (1978) *Phys Stat Sol A* 45:359
9. Aleshin AN, Bokstein BS, Shvindlerman LS (1977) *Sov Phys Sol State* 19:3511
10. Gottstein G, Shvindlerman LS (2009) *Grain boundary migration in metals: thermodynamics, kinetics, applications*. CRC Press Inc, Boca Raton
11. Tan TY, Sass SL, Balluffi RW (1975) *Phil Mag* 31:575
12. Straumal BB, Shvindlerman LS (1985) *Acta Metall* 33:1735
13. Straumal BB, Klinger LM, Shvindlerman LS (1984) *Acta Metall* 32:1355
14. Molodov DA, Straumal BB, Shvindlerman LS (1984) *Scr Metall* 18:207
15. Aleshin AN, Prokofiev SI, Shvindlerman LS (1985) *Scr Metall* 19:1135
16. Hsieh TE, Balluffi RW (1989) *Acta Metall* 37:2133
17. Kim MJ, Cho YK, Yoon DY (2004) *J Am Ceram Soc* 87:455
18. Rottman C, Wortis M (1984) *Phys Rev B* 29:328
19. Straumal BB, Semenov VN, Kogtenkova OA et al (2004) *Phys Rev Lett* 192:196101
20. Keshishev KO, Parshin AY, Babkin AV (1981) *Sov Phys JETP* 53:362
21. Maksimova EL, Shvindlerman LS, Straumal BB (1988) *Acta Metall* 36:1573
22. Maksimova EL, Shvindlerman LS, Straumal BB et al (1989) *Acta Metall* 37:2855
23. Maksimova EL, Rabkin EI, Shvindlerman LS et al (1989) *Acta Metall* 37:1995
24. Kinoshita Y, Yardley VA, Tsurekawa S (2011) *J Mater Sci* 46:4261. doi:[10.1007/s10853-010-5241-6](https://doi.org/10.1007/s10853-010-5241-6)
25. Kurihara K, Kokawa H, Sato S et al (2011) *J Mater Sci* 46:4270. doi:[10.1007/s10853-010-5244-3](https://doi.org/10.1007/s10853-010-5244-3)
26. Figueiredo RB, Langdon TG (2010) *J Mater Sci* 45:4827. doi:[10.1007/s10853-010-4589-y](https://doi.org/10.1007/s10853-010-4589-y)
27. Baretzky B, Friesel M, Petelin A et al (2006) *Def Diff Forum* 258:397
28. Duparc OBMH (2011) *J Mater Sci* 46:4116. doi:[10.1007/s10853-011-5367-1](https://doi.org/10.1007/s10853-011-5367-1)
29. Semenov VN, Straumal BB, Glebovsky VG et al (1995) *J Cryst Growth* 151:180
30. Schölhammer J, Baretzky B, Gust W et al (2001) *Interf Sci* 9:43
31. Straumal BB, Polyakov SA, Mittemeijer EJ (2006) *Acta Mater* 54:167
32. Kogtenkova O, Straumal B, Protasova S et al (2005) *Zt Metallkd* 96:216
33. Straumal BB, Semenov VN, Kogtenkova OA et al (2004) *Phys Rev Lett* 192:196101
34. Straumal BB, Sursaeva VG, Polyakov SA (2001) *Interface Sci* 9:275
35. Straumal BB, Polyakov SA, Bischoff E et al (2001) *Interface Sci* 9:287
36. Straumal B, Polyakov S, Bischoff E et al (2004) *Zt Metallkd* 95:939
37. Kogtenkova OA, Straumal BB, Protasova SG et al (2005) *Def Diff Forum* 237:603
38. Protasova SG, Kogtenkova OA, Straumal BB (2007) *Mater Sci Forum* 558:949
39. Gallagher PCJ (1970) *Metall Trans* 1:2429
40. Chang L-S, Rabkin E, Straumal BB et al (1998) *Defect Diff Forum* 156:135
41. Straumal BB, Polyakov SA, Bischoff E et al (2003) *Def Diff Forum* 216:93
42. Straumal BB, Polyakov SA, Chang L-S et al (2007) *Int J Mater Res (Zt Metallkd)* 98:451
43. Gokon N, Kajihara A (2008) *Mater Sci Eng A* 477:121
44. Goukon N, Yamada T, Kajihara M (2000) *Acta Mater* 48:2837
45. Lojkowski W, Sodervall U, Mayer S (1998) *Interface Sci* 6:187
46. Kuhn H, Bäro G, Gleiter H (1979) *Acta Metall* 27:959
47. Goodhew PJ, Tan TY, Balluffi RW (1978) *Acta Metall* 26:557
48. Wolf U, Ernst F, Muschik T et al (1992) *Phil Mag A* 66:991
49. Ernst F, Finnis MW, Hoffmann D et al (1992) *Phys Rev Lett* 69:620
50. Hofmann D, Finnis MW (1994) *Acta Metall Mater* 42:3555
51. Straumal B, Sursaeva V, Baretzky B (2010) *Scr Mater* 62:924
52. Heyraud JC, Metois JJ (1980) *Acta Metal* 28:1789
53. Heyraud JC, Metois JJ (1983) *Surf Sci* 128:334
54. Mullins WW (1956) *Acta Metall* 4:421
55. Dingley DJ, Pond RC (1979) *Acta Metall* 27:667
56. Pegel B (1968) *Phys Status Solid* 28:603
57. Rybin VV, YuF Titovets, Teplitsky DM, Zolotarevsky NYu (1982) *Fiz Metall Metalloved* 53:544 (in Russian)
58. Davidson D, den Nijs M (2000) *Phys Rev E* 59:5029
59. Davidson D, den Nijs M (2000) *Phys Rev Lett* 84:326
60. Wynblatt P, Chatain D (2009) *Rev Adv Mater Sci* 21:44
61. Chatain D, Ghetta V, Wynblatt P (2004) *Interface Sci* 12:7
62. Saka H, Iwata T, Imura T (1978) *Phil Mag A* 37:273
63. Shin K, King AH (1991) *Phil Mag A* 63:1023
64. Chen F-R, King AH (1988) *Acta crystallogr B* 43:416
65. Straumal BB, Gornakova AS, Sursaeva VG (2008) *Phil Mag Lett* 88:27